Electronic Supplementary Material (ESI) for Physical Chemistry Chemical Physics.

Supplementary Information - Resolving Structures of Transition Metal Complex Reaction Intermediates with Femtosecond EXAFS

Alexander Britz[1,2,*], Baxter Abraham[3], Elisa Biasin[1], Tim Brandt van Driel[2], Alessandro Gallo[4], Angel T. Garcia-Esparza[3], James Glownia[2], Anton Loukianov[2], Silke Nelson[2], Marco Reinhard[1], Dimosthenis Sokaras[3,*] and Roberto Alonso-Mori[2,*]

[1]Stanford PULSE Institute, SLAC National Accelerator Laboratory, Menlo Park, CA 94025, USA

[2]Linac Coherent Light Source, SLAC National Accelerator Laboratory, Menlo Park, CA 94025, USA

[3]Stanford Synchrotron Radiation Lightsource, SLAC National Accelerator Laboratory, Menlo Park, CA94025, USA

[4]SUNCAT Center for Interface Science and Catalysis, Department of Chemical Engineering, Stanford University, Stanford, CA94305 and SLAC National Accelerator Laboratory, Menlo Park, CA94025, USA

*abritz@slac.stanford.edu

*dsokaras@slac.stanford.edu

*robertoa@slac.stanford.edu

1. Deglitching and Filtering of Data

In the measurement we have determined two sources of artifacts (=glitches), and prior to analyzing the spectra these points have been removed. One large hump-like feature around 7.35 keV is expected to be due to scattering from an obstacle, as it is not present in a simultaneous measurement with a PIBS diode on the opposite side of the jet (see Fig. S1 left). Furthermore, several very sharp features consisting of few points are visible in the spectrum. These appear at energies, at which few events are acquired (see Fig. S2), and consequently, these points are removed as well.
Fig. S3 shows a comparison of the (100±100) fs raw data, the re-binned, in which two neighboring energy points are averaged and the filtered data using a Savitzky-Gollay filter with 11 point window size and third order polynomial.

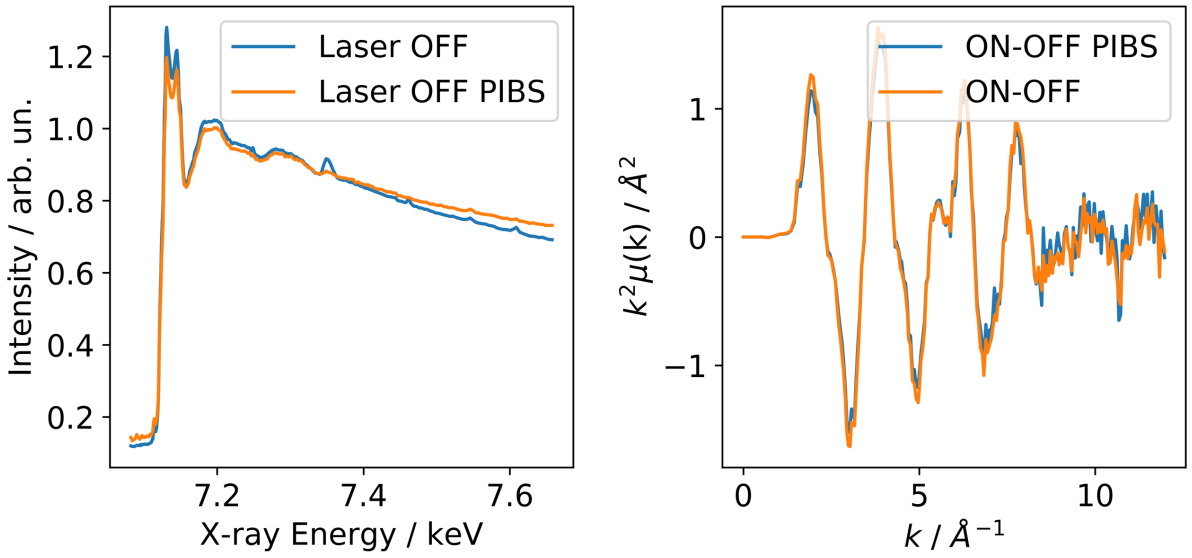

Figure S1: Left: Ground state EXAFS measured with ePIX compared to PIBS diode measurement. The artifact around 7.35 keV is only visible in the ePIX measurement. Right: Comparison of transient differences measured with both detection methods.

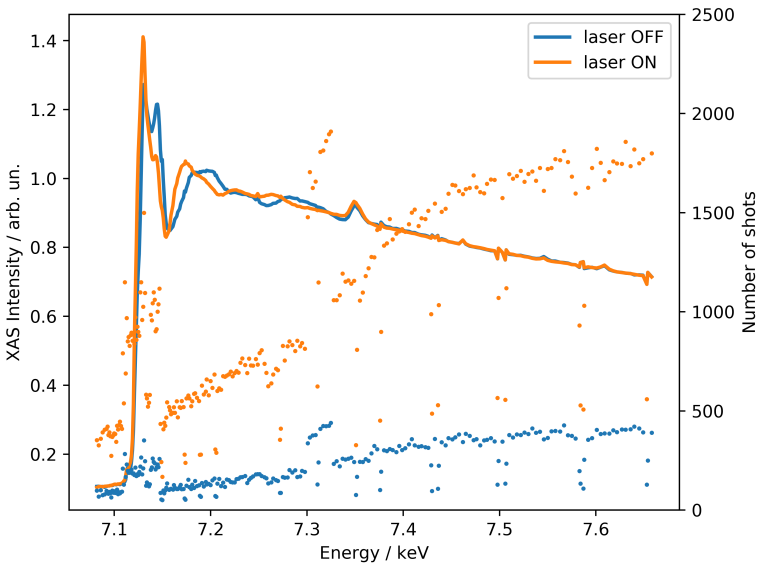

Figure S2: EXAFS spectra of GS and 10 ps after photoexcitation together with the number of X-ray pulses acquired for each energy point. The glitches in the spectrum are found at points, where significantly fewer pulses are acquired than at the neighboring points.

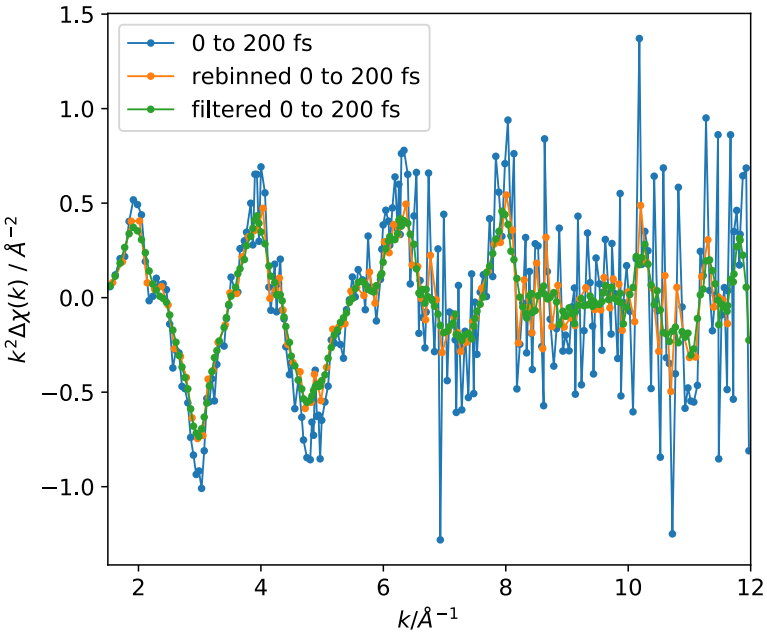

Figure S3: Comparison of raw, re-binned and filtered data.

2. Comparison of Low vs. High Laser Excitation Power

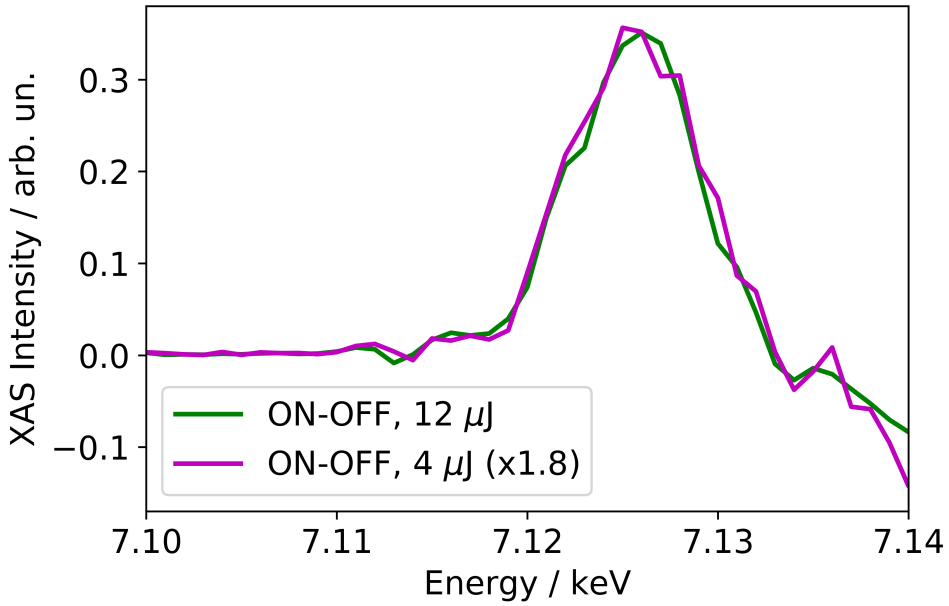

Figure S4: Comparison between low (4 μJ) and high (12 μJ) laser excitation pulse energy. The transient difference at both energies is qualitatively identical.

3. Details on EXAFS Fit and Simulation

3.1. Summary of experimentally and theoretically determined structures of $[Fe(terpy)_2]^{2+}$ from literature

Summary of experimentally and theoretically determined structures of $[Fe(terpy)_2]^{2+}$. Here the first coordination shell interatomic distances are labeled r_{Nax} and r_{Neq} for the Fe bond with the axial and equatorial N (N_{ax} and N_{eq}), respectively. The C in the second coordination shell form three groups, C_{ax}, C_{eq1} and C_{eq2}, which each consist of 4 equivalent Fe-C distances. The structures of the LS ground state, the long-lived HS excited state and the potential short-lived IS state have been modeled by Jakubikova *et al*. using DFT.[1] Experimentally the interatomic distances of the LS and HS states have been determined via EXAFS measurements at synchrotrons and those from two different publications are listed.[2,3]

Table S2: Summary of experimentally and theoretically determined Fe-N and Fe-C interatomic distances in $[Fe(terpy)_2]^{2+}$

	r_{Nax} / Å	r_{Neq} / Å	r_{Cax} / Å	r_{Ceq1} / Å	r_{Ceq2} / Å
LS DFT[1]	1.91	2.00	2.82	2.84	3.01
IS DFT[1]	1.94	2.14	2.86	2.94	3.15
HS DFT[1]	2.16	2.20	3.06	3.14	3.17
LS Synchrotron [2]	1.86±0.02	1.97±0.02	2.80±0.03	2.83±0.02	2.99±0.03
HS Synchrotron [2]	2.09±0.02	2.18±0.02	2.98±0.02	3.02±0.02	3.18±0.02
LS Synchrotron [3]	1.874±0.004	1.969±0.02			
HS Synchrotron [3]	2.08±0.02	2.20±0.01			

3.2. EXAFS Simulation and Fit Results

The EXAFS has been optimized in the *k*-range of 2.5 $Å^{-1}$ to 10.5 $Å^{-1}$ and an R-range of 1 Å to 4.5 Å. The fits presented in this publication were performed in R-space, the respective fits in k-space lead to, within the error bars, very similar results (especially of the obtained interatomic distances). In the EXAFS fit performed in ARTEMIS, apart from the atomic distances, the following parameters are optimized: The amplitude reduction factor S_0^2, an energy shift ΔE_0, as well as two Debye-Waller factors σ^2_N and σ^2_C for the first coordination shell N and the second coordination shell C, respectively. We have included ~50 further scattering paths, which consist of single scattering of C atoms at longer distances as well as multiple scattering paths (e.g. triangles, double forward scattering, etc.). The σ^2_{rest} for all other scattering paths is set to the sum $\sigma^2_N + \sigma^2_C$ and their respective length has been optimized with a global correction. As the initial guesses, the DFT structures from literature[1] have been used. In the GS fit, the correction of R_{Nax} was locked to the one of R_{Neq} and all three Fe-C interatomic distances were optimized together, in order to reduce the number of fit parameters. In the ES, the σ^2 and S_0^2 were fixed to the values obtained from the GS fit and all other parameters were optimized. This fit procedure has already been used in literature.[3,4]

Table S2: Details of EXAFS fit and simulations

Description	#	R_{Nax} / Å	R_{Neq} / Å	R_{Cax} / Å	R_{Ceq1} / Å	R_{Ceq2} / Å	S_0^2	E_0	σ_N^2 / 10^{-3} Å^2	σ_C^2 / 10^{-3} Å^2	σ_{rest}^2 / 10^{-3} Å^2	χ^2
GS Fit	1	1.86 ±0.02	1.96 ±0.02	2.76 ±0.05	2.84 ±0.05	2.94 ±0.05	0.70 ±0.07	7122.7 ±1.0	3.5 ±1.5	3.9 ±2.6	7.3 ±4.1	1204
ES Fit	2	2.08 ±0.02	2.17 ±0.02	2.97 ±0.03	3.02 ±0.03	3.11 ±0.03	0.70	7124.5 ±0.6	3.5	3.9	7.3	875
$^1A_1$ Simulation	3	1.86	1.95	2.79	2.79	2.95	0.70	7122.7	3.5	3.9	7.3	
$^3T_1$ Simulation	4	1.89	2.09	2.83	2.90	3.12	0.70	7122.7	3.5	3.9	7.3	
$^5T_2$ Sim. (hot)	5	2.11	2.16	3.03	3.03	3.12	0.70	7122.7	7.0	7.8	14.6	
$^5T_2$ Sim. (cold)	6	2.11	2.16	3.03	3.03	3.12	0.70	7122.7	3.5	3.9	7.3	

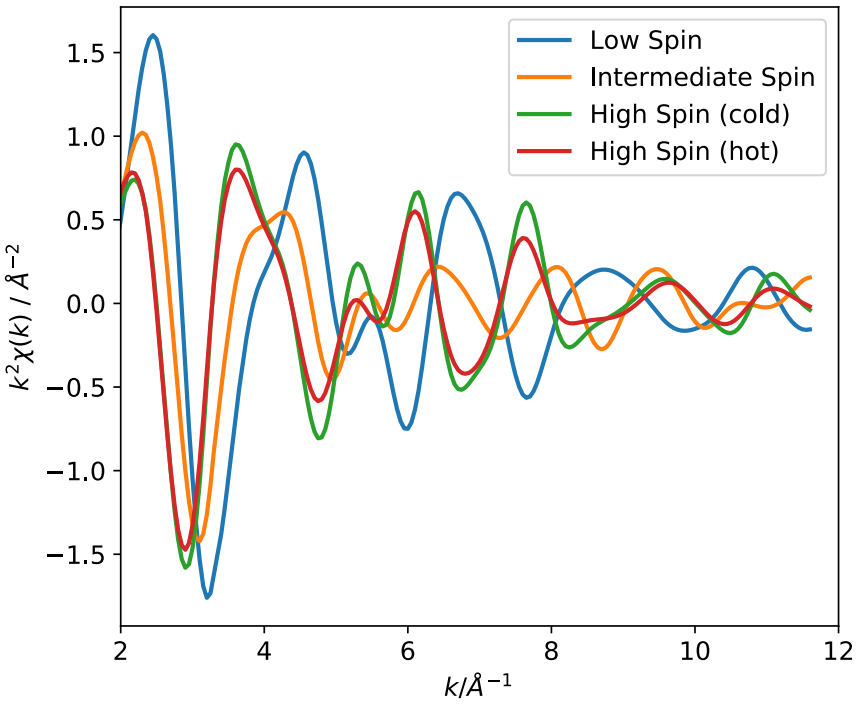

Figure S5: EXAFS simulation with Feff6 of the low spin ground state, the short-lived intermediate spin state as well as the hot and cold the ns-lived high spin state (see Table S2 #3-6 for details)

4. Estimating the Relative Short-lived Intermediate State Population

We simulated the excited populations of a simple model including 3 species, the $^1A_1$ ground state, the short-lived triplet intermediate (^3T) and the long-lived $^5T_2$ quintet, see Ref[5] for detailed explanations on the kinetic models for the example of $[Fe(bpy)_3]^{2+}$. The MLCT intermediate state is neglected here.

$$^1A_1 \rightarrow {}^3T \rightarrow {}^5T_2 \rightarrow {}^1A_1$$

Furthermore, we assumed a 100-fs-lifetime of the ^3T species, and a 2.6 ns lifetime for the $^5T_2$ state. Additionally, we used a Gaussian instrument response function of 70 fs FWHM, which consists of the group velocity mismatch in the 50 µm thick liquid jet and the pulse width of the optical pump laser and the X-ray probe.

The relative ^3T population in the interval -100 fs to 100 fs is 57 %, while in the range 100 fs to 300 fs it is only 18 %.

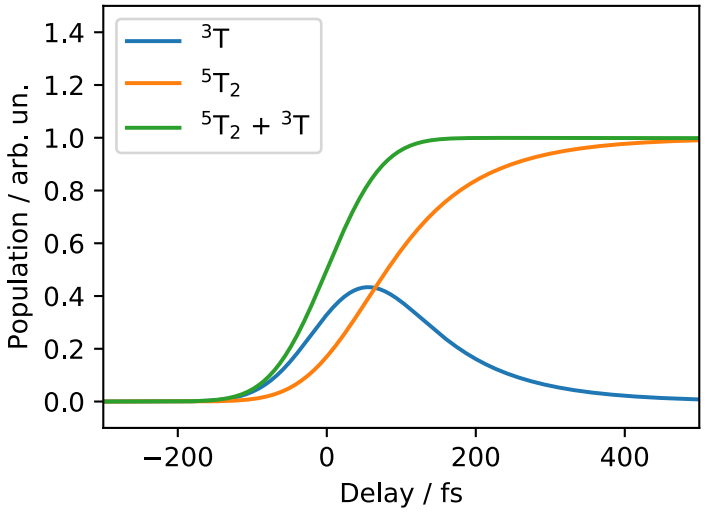

Figure S6: Population of excited states in a kinetic model with 3 species.

5. Synthesis of $[Fe(terpy)_2]^{2+}Cl_2$

$[Fe(terpy)_2]^{2+}Cl_2$ was synthesized following standard procedures from literature.[6,7] 0.47 g terpyridine were dissolved in 10 mL Ethanol, 0.2 g $FeCl_2{:}4H_20$ in ~4 mL Ethanol. The terpyridine solution was stirred and the $FeCL_2$ solution was added, resulting in a purple mixture, indicating the formation of $[Fe(terpy)_2]^{2+}$. The solution was heated to ~50° C for to ~1 h. Crystallization was achieved by further addition of hexane. The sample was filtered and rinsed with hexane. Characterization with NMR and UV-vis absorption spectroscopy verified the formation of the $[Fe(terpy)_2]^{2+}Cl_2$.

6. Femtosecond Transient XAS Spectra in Energy Space

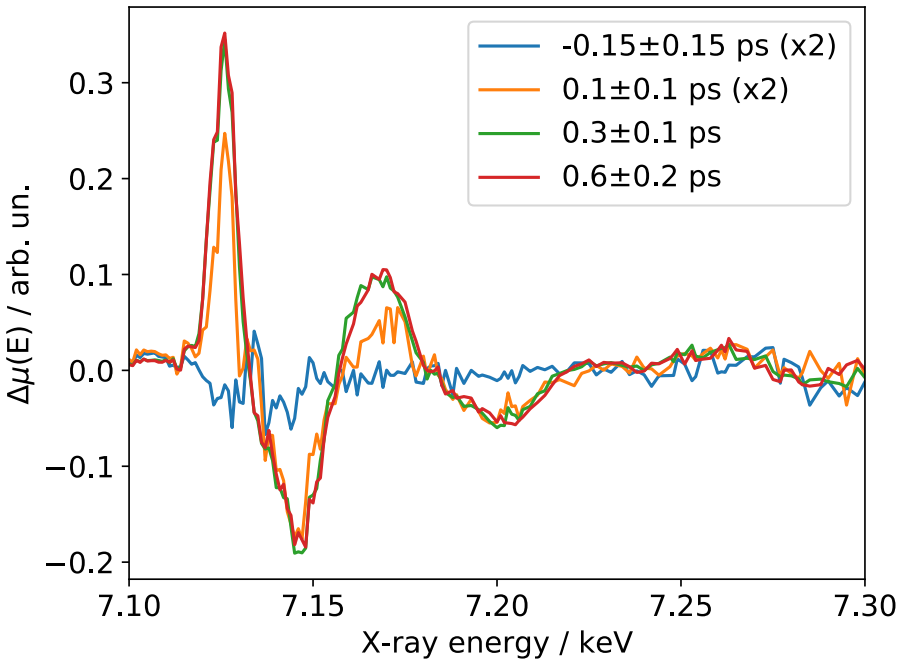

Figure S7: Femtosecond transient XAS spectra in energy space at four different pump-probe delays.

References

1 D. N. Bowman, A. Bondarev, S. Mukherjee and E. Jakubikova, *Inorg. Chem.*, 2015, **54**, 8786–8793.

2 X. Zhang, M. L. Lawson Daku, J. Zhang, K. Suarez-Alcantara, G. Jennings, C. A. Kurtz and S. E. Canton, *J. Phys. Chem. C*, 2015, **119**, 3312–3321.

3 G. Vankó, A. Bordage, M. Pápai, K. Haldrup, P. Glatzel, A. M. March, G. Doumy, A. Britz, A. Galler, T. A. Assefa, D. Cabaret, T. B. Van Driel, K. S. Kjær, A. O. Dohn, K. B. Moller, H. T. Lemke, M. Rovezzi, Z. Németh, E. Rozsályi, T. Rozgonyi, J. Uhlig, V. Sundstrom, M. M. Nielsen, L. Young, S. H. Southworth, C. Bressler and W. Gawelda, *J. Phys. Chem. C*, 2015, **119**, 5888–5902.

4 A. Britz, W. Gawelda, T. A. Assefa, L. L. Jamula, J. T. Yarranton, A. Galler, D. Khakhulin, M. Diez, M. Harder, G. Doumy, A. M. March, É. Bajnóczi, Z. Németh, M. Pápai, E. Rozsályi, D. S. Szemes, H. Cho, S. Mukherjee, C. Liu, T. K. Kim, R. W. Schoenlein, S. H. Southworth, L. Young, E. Jakubikova, N. Huse, G. Vankó, C. Bressler and J. K. McCusker, *Inorg. Chem. (in press).*

5 W. Zhang, R. Alonso-Mori, U. Bergmann, C. Bressler, M. Chollet, A. Galler, W. Gawelda, R. G. Hadt, R. W. Hartsock, T. Kroll, K. S. Kjær, K. Kubiček, H. T. Lemke, H. W. Liang, D. a Meyer, M. M. Nielsen, C. Purser, J. S. Robinson, E. I. Solomon, Z. Sun, D. Sokaras, T. B. van Driel, G. Vankó, T.-C. Weng, D. Zhu and K. J. Gaffney, *Nature*, 2014, **509**, 345–348.

6 J. K. McCusker, A. L. Rheingold and D. N. Hendrickson, *Inorg. Chem.*, 1996, **35**, 2100–2112.

7 V. V. Avdeeva, A. V. Vologzhanina, L. V. Goeva, E. A. Malinina and N. T. Kuznetsov, *Zeitschrift für Anorg. und Allg. Chemie*, 2014, **640**, 2149–2160.